Published in final edited form as:
Dev Biol. 2013 January 15; 373(2): 281–289. doi:10.1016/j.ydbio.2012.11.009.

Whole-organ cell shape analysis reveals the developmental basis of ascidian notochord taper

Michael T. Veeman[**,1] and **William C. Smith**[*]
Department of Molecular, Cell and Developmental Biology, and Neuroscience Research Institute, University of California Santa Barbara, Santa Barbara, California 93106, United States

Abstract

Here we use *in toto* imaging together with computational segmentation and analysis methods to quantify the shape of every cell at multiple stages in the development of a simple organ: the notochord of the ascidian *Ciona savignyi*. We find that cell shape in the intercalated notochord depends strongly on anterior-posterior (AP) position, with cells in the middle of the notochord consistently wider than cells at the anterior or posterior. This morphological feature of having a tapered notochord is present in many chordates. We find that ascidian notochord taper involves three main mechanisms: Planar Cell Polarity (PCP) pathway-independent sibling cell volume asymmetries that precede notochord cell intercalation; the developmental timing of intercalation, which proceeds from the anterior and posterior towards the middle; and the differential rates of notochord cell narrowing after intercalation. A quantitative model shows how the morphology of an entire developing organ can be controlled by this small set of cellular mechanisms.

Keywords

Ciona; Notochord; Morphogenesis; Morphometrics

Introduction

Embryonic morphogenesis involves the fine spatial and temporal control of many cell parameters, including numerous aspects of cell shape and motility. The ascidian *Ciona* has a stereotyped chordate body plan with a notochord and hollow dorsal neural tube in the context of an embryo small enough to be imaged *in toto* in a single field of view at high resolution. This has led to the emergence of *Ciona* and related ascidian species as model systems for image-based, quantitative studies of chordate morphogenesis *in toto* (Munro and Odell, 2002; Sherrard et al., 2011; Tassy et al., 2006).

Manual image segmentation in 3D involves the laborious tracing of cell outlines in all of the planes of an image stack, and can rapidly become prohibitively time-consuming for more than a modest number of cells. Automated 2D segmentation methods have recently become powerful tools for high throughput image-based screening of cultured cells (e.g. (Carpenter

[*]Corresponding author.Tel.: +1 805 893 3883; fax: +1 805 893 2005. william.smith@lifesci.ucsb.edu. [**]Corresponding author. veeman@ksu.edu.
[1]Current address: Division of Biology, Kansas State University, Manhattan, Kansas, USA

et al., 2006; Thomas, 2009), but fully automated 3D segmentation tools are still being developed e.g. (Dufour et al., 2005; Zanella et al., 2009). Here we take a middle path, using an interactive, semi-automated method to segment more than 2000 ascidian notochord cells in 3D.

The ascidian notochord consists of exactly 40 cells that intercalate to form a single-file column that acts as a stiffening element in the center of the tail (Munro et al., 2006). The notochord is one of the defining features of the chordate body plan and, although transient in many species, is typically the first organ to develop (Stemple, 2005). The cell lineages for the ascidian notochord are well established, though there is known to be a transition from completely stereotyped to partially stochastic cell behaviors during notochord cell intercalation (Nishida, 1987). After intercalation is complete, the notochord cells change from being shaped like thin, flat disks to become longer in the anterior to posterior dimension and narrower in the mediolateral dimension (Miyamoto and Crowther, 1985). This process is poorly understood, but is known to involve actomyosin contractility (Dong et al., 2011; Dong et al., 2009). The notochord cells subsequently undergo complex rearrangements that result in them forming an inflated hollow tube running the length of the tail (Dong et al., 2011; Dong et al., 2009).

Our initial goal was to quantify the 3D shape of every notochord cell from the end of intercalation until the onset of tubulogenesis, so as to determine how cell shape varies both spatially within the embryo and temporally from stage to stage. Upon identifying an extremely consistent taper in the intercalated notochord from a wide middle towards narrower tips, we then switched from discovery-driven to hypothesis-driven experiments to determine the cellular mechanisms underlying this phenomenon.

Materials and Methods

Imaging

Ciona savignyi eggs were fertilized and dechorionated by standard methods (Veeman et al.). Embryos were fixed in 2% EM grade paraformaldehyde in seawater, stained with Bodipy-FL phallacidin (Molecular Probes), cleared through an isopropanol series and mounted in Murray Clear (1:2 benzyl alcohol and benzyl benzoate). They were imaged on an Olympus Fluoview 1000 laser scanning confocal using a 40× 1.3na objective. Images were collected with a voxel size of 155 nm in X and Y, and 300 nm in Z.

Staging

The timepoints examined were more closely spaced than the stages of the standard *Ciona* staging series of Hotta (Hotta et al., 2007), so we have presented timepoints as actual minutes of development using the first timepoint in each dataset as t=0. Approximate Hotta stages are also given for comparison between datasets. Each of our three main time series datasets (post-intercalation, during intercalation and wt versus *aim*) was generated from a single fertilization with a narrow 10 minute fertilization window, giving rise to extremely synchronized embryos. All embryos were grown at approximately 18°C.

Marker Generation

Initial testing showed that marker-assisted watershed produced a good segmentation of notochord cell boundaries. Two types of markers were used: a short line inside each notochord cell and a rough shell around the outside of the notochord. The outer shell did not need to be particularly close to the notochord, but it needed to intersect all of the notochord's neighboring cells without intersecting the notochord itself.

Although a significant improvement over manually tracing the outline of every notochord cell, hand drawing the outer shell remained laborious as it required a rough outline to be drawn in hundreds of Z slices. To address this problem, we took advantage of the essentially curvilinear sausage-like shape of the notochord, which can be approximated by fitting a spline to its midline together with a value for the radius at each point on the spline. This can be thought of as the Minkowski sum of the midline spline dilated by a sphere of varying radius. As the notochord is locally quite smooth, only a small number of control points are required to achieve a good approximation by cubic spline interpolation. We implemented a Matlab GUI that allows the user to make a small number of line selections in a 3D slice browser and then builds the Minkowski sum accordingly. New control points can be added interactively to refine the mask as needed, with a typical image requiring one at each end of the notochord and 3-4 in the middle.

The GUI also allows the user to generate the inner markers by making a line selection in the center of each cell. A line across the nucleus was found to give a more consistent segmentation than a point, as it spanned the perinuclear actin blobs that otherwise occasionally perturbed the segmentation.

Cell Segmentation

Image volumes were resized by cubic spline interpolation to give isotropic 0.3 μm voxel sizes, and then smoothed by coherence enhancing diffusion (CED) (Weickert, 1999) using the implementation by Kroon and Slump (Kroon and Slump, 2009) modified to enhance planar rather than curvilinear features. Notochord cells were segmented by the seeded watershed transform (Meyer and Beucher, 1990; Vincent and Soille, 1991), using markers interactively generated as discussed above. The seeded watershed algorithm then propagates away from those markers to identify the notochord cell boundaries. When necessary, the markers were manually refined until an acceptable segmentation was achieved. The algorithm returns a label matrix L in which the voxels belonging to each of J watershed domains are labeled $1\ldots J$, and the watershed surfaces between domains are labeled 0. For convenience, we reorder the label matrix so that the index j=1 for the anteriormost cell through j=40 for the posteriormost cell, with the "not-notochord" segment labeled j=41.

Cylindrical model fitting

For post-intercalation stages, we fitted a cylindrical model to each cell to robustly measure height and diameter in three dimensions. Principal component analysis (PCA) was used to identify the cylinder axis, now denoted $\widehat{\mathbf{e}}_{\mathrm{cyl}}$, of each cell as the eigenvector best aligned with the vectors between that cell's centroid **c** and its anterior and posterior neighbors. For each cell j we used binary morphology to subsegment it into its anterior and posterior surfaces (the tops and bottoms of the cylinder, which contact other notochord cells) and its lateral surfaces (the sides of the cylinder, which contact the flanking tissues).

$$\begin{aligned} L_j^{\mathrm{lat}} &= \left(L_j \oplus B\right) \cap \left(L_{41} \oplus B\right) \\ L_j^{\mathrm{ap}} &= \left(L_j \oplus B\right) \cap \left(L_{j+1} \oplus B\right) \cup \left(L_j \otimes B\right) \cap \left(L_{j-1} \oplus B\right) \end{aligned}$$

(where B is a 3×3×3 structuring element and $\oplus$ is binary dilation)

Mean height was measured by calculating twice the mean of the closest distance from each point in the anterior and posterior surfaces to a plane through the cell centroid orthogonal to the cylinder axis.

$$\bar{h} = \sum_{m=1}^{M} \frac{2\left|\widehat{\mathbf{e}}_{\mathbf{cyl}} \cdot (\mathbf{c} - \mathbf{q}_m)\right|}{M} \quad \text{for} \quad \mathbf{q}_m = \begin{bmatrix} x_m \\ y_m \\ z_m \end{bmatrix} \in L_j^{\text{ap}}$$

Mean radius was measured by calculating the mean of the closest distance from each point in the lateral surfaces to a line defined by the cell centroid and the cylinder axis.

$$\bar{r} = \sum_{k=1}^{K} \frac{\left\|\widehat{\mathbf{e}}_{\mathbf{cyl}} \times (\mathbf{c} - \mathbf{p}_k)\right\|}{K} \quad \text{for} \quad \mathbf{p}_k = \begin{bmatrix} x_k \\ y_k \\ z_k \end{bmatrix} \in L_j^{\text{lat}}$$

Scripts for these analyses were all implemented in Matlab. As the first and last notochord cells are shaped more like bullets than cylinders, they were excluded.

Microsurgery

For tail cut experiments the tail was cut in half at its approximate mid point using a fine glass needle. The resulting fragments were gently moved apart so they did not reattach and then cultured for two hours before being fixed, stained and imaged.

Intercalation Timing

Each cell was manually scored as being intercalated if its contacts with non-notochord cells formed a closed ring, and not intercalated if these contacts formed only a segment of arc. For this series of images, we measured notochord diameter manually in ImageJ by fitting circular regions of interest (ROIs) to orthogonal notochord cross-sections resliced at a given cell position.

Notochord taper in other chordates

Notochord taper was examined in lamprey and amphioxus larvae using commercial prepared specimens, and in zebrafish larvae kindly provided by Jungho Kim and Michael Liebling. Tiled images were mosaiced using the Photomerge utility in Adobe Photoshop.

Modeling notochord taper

All models were implemented in Matlab, using the formulas discussed later. All results are normalized to have a mean radius of 1.

Results

The *Ciona* notochord is tapered towards both ends

We imaged the notochord by confocal microscopy *in toto* and at high resolution in five Bodipy-FL phallacidin stained embryos fixed at each of nine timepoints. These timepoints span a three-hour period after the notochord cells have intercalated during which they undergo a dramatic change in aspect ratio, becoming progressively taller in the anterioposterior dimension and narrower in the mediolateral dimension. The notochord cells are all roughly cylindrical during this period, but change from disk-shaped to drum-shaped. This cell shape change, which we call the disk-to-drum transition, accounts for much of the overall elongation of the tail (Figure 1A).

After segmenting all of the notochord cells in this dataset, we fitted a cylindrical model to each cell, allowing us to make robust measurements of average height (the AP dimension)

and diameter (the mediolateral dimension). These measurements were all made in 3D and are not subject to the artefacts that can occur if measurements are made on a single 2D plane that slices obliquely across a 3D object. Figure 1A shows a single confocal plane across the notochord in a representative embryo at each timepoint, with the segmentation overlayed as random pseudocolors. Supplementary Movie 1 shows an example of an original image stack, and Supplementary Movies 2-4 show 3D renderings of segmented notochord cells in progressively older embryos.

As shown in Figure 1B, notochord cell height increases during this time period, whereas notochord cell diameter decreases. Despite the extremely stereotyped nature of *Ciona* development, there is considerable spread in the values for both height and diameter at a given timepoint, with diameter being particularly broadly distributed. Most of this variation in height and width is a function of AP position within the embryo, as shown in Figure 1C for all 5 embryos at the 45 minute timepoint. Cells in the middle of the notochord are much wider than cells at either end, with cells at the anterior end somewhat wider than cells at the posterior end. Cells are tallest in the front of the notochord, but this relationship is less pronounced. We generally did not see any sharp transitions in height or width between the anterior 32 'primary' notochord cells versus the posterior 8 'secondary' notochord cells that are derived from a different embryonic lineage (Nishida, 1987).

This basic pattern of notochord cells being widest in the middle of the notochord and narrowest at the ends is evident at all of the stages examined (Figure 1D). To examine the relative sizes of cells in embryos of different stages, we normalized notochord cell diameter to the mean notochord cell diameter in each embryo (Figure 1E). This revealed that the relative diameter of the notochord as a function of AP position is stable over this time period despite the dramatic cell shape changes of the disk-to-drum transition. This scaling property implies that the rate of notochord cell narrowing is a function of notochord cell diameter, and can thus be modeled as an exponential decrease.

We fit exponential models to the data to estimate the narrowing rate from anterior to posterior in terms of the 'halving time' required for a particular cell position to narrow by ½ (Figure 1F). Halving times are roughly constant over much of the notochord but are somewhat higher for the first and last ~5 cells. This indicates that taper decreases slightly over time, as the ends undergo the disk-to-drum transition slower than the middle, although not enough to be apparent in plots of normalized taper such as Figure 1E. The notochord's characteristic taper must therefore emerge before or during intercalation, and we can exclude the possibility that taper might emerge after intercalation through cells at the ends of an initially straight notochord narrowing faster than cells in the middle.

Notochord taper is widespread in the chordates

To determine if notochord taper is a conserved aspect of chordate body plans, we examined larval specimens of zebrafish (a higher vertebrate), lamprey (at the base of the vertebrate lineage) and *Amphioxus* (another invertebrate chordate). In all three organisms, the notochord showed a similar taper towards both the anterior and the posterior (Figures 2A, 2B and 2C). To the best of our knowledge, the embryological basis for notochord taper has not been previously addressed.

A bisected tail does not reestablish a new taper

One hypothesis for the origin of ascidian notochord taper is that it might reflect the balance of mechanical forces such as contractility and adhesion (Montell, 2008; Paluch and Heisenberg, 2009) for a column of disk-shaped cells and their associated perinotochordal basement membrane (Veeman et al., 2008), acting over a very short timescale. One could

imagine that such an arrangement of cells might naturally and rapidly form a tapered shape through the combined effects of cortical cell contractility, cell-cell adhesion, and the mechanical properties of the associated extracellular matrix. We tested this model by cutting ascidian tails in half shortly after the end of notochord intercalation. The resulting fragments quickly healed and continued to elongate and undergo the disk-to-drum transition, but the new anterior and posterior ends remained blunt and a new taper was not reestablished (Figure 3). This experiment is subject to certain caveats about the forces generated or released by the tail cut, and the nature of the wound healing process, but it supports the idea that taper is established before or during intercalation. We conclude that taper must represent more than the short-timescale biophysics of a column of disk-shaped cells.

Ciona notochord cells intercalate from the ends towards the middle

Another potential mechanism involves developmental timing. The disk-to-drum transition occurs after intercalation is complete and makes the notochord narrower. If intercalation progressed from the ends of the notochord towards the middle, this would give the anterior and posterior cells a ‘head start’ on their subsequent change in aspect ratio, giving rise to taper. The timing of notochord cell intercalation had not previously been described, so we imaged 4 embryos fixed at each of 6 timepoints during intercalation and scored each notochord cell as being either intercalated or not. While there was embryo-to-embryo variation in the precise timing of intercalation, the clear trend is that the notochord does intercalate from its ends towards its middle (Figures 4A, 4B, 4C and 4D). This pattern of mediolateral intercalation seems logical, in that cells at the front and back of the disk-shaped notochord primordium have less distance to travel and require fewer neighbor exchanges to complete intercalation (Figures 4E and 4F).

We also measured the diameter of the entire notochord (representing more than one cell in cross-section if intercalation was not yet complete at that position) at three AP positions: near the anterior (cell 3), the middle (cell 16) and the posterior (cell 38) (Figure 4G). We estimated the mean width of each cell at the moment intercalation is completed by fitting a simple exponential model and interpolating the diameter at the time when a given cell has a 50% probability of being fully intercalated. We used an exponential rather than a linear function because, as discussed later, the disk-to-drum transition can be modeled as an exponential decrease in radius. These results suggest that cell 3 and cell 16 have similar diameters at the moment of intercalation (21.2 μm vs 21.6 μm, 95% confidence intervals of the model fit: 18.9 μm-23.4 μm vs 18.0 μm-25.2 μm) and that much of the difference in diameter between them at post-intercalation stages results from cell 3 intercalating much earlier than cell 18. Cell 38, however, is estimated to be considerably narrower at the moment of intercalation (14.1 μm, 95% confidence interval: 11.8 μm-16.5 μm). Using the Delta method for the variance of quotients, we estimate with 95% confidence that between 31-100% of the difference in diameter between cell 3 and cell 16 is due to cell 3 intercalating first and thus having a head start on the disk-to-drum transition. For cell 38, however, the head start accounts for only 0-38% of its reduced diameter relative to cell 16.

Despite these relatively broad confidence intervals, developmental timing clearly plays an important role in the establishment of notochord taper, as indeed it must if cells complete intercalation and begin the disk-to-drum transition from the ends towards the middle. This timing cannot, however, be the only mechanism at work. This is particularly evident for the posteriormost cells, which intercalate more slowly than the anteriormost cells but are narrower after intercalation.

Asymmetries in cell volume

Another potential mechanism is that notochord cells may differ in volume even before intercalation. To test this, we segmented the notochord cells in embryos fixed very early in intercalation, shortly after the final cell divisions of most of the notochord lineage (Figures 5A, 5B and 5C). By plotting cell volume as a function of anterior-posterior position within the disk-shaped notochord primordium, we found that there was indeed a relationship, with cells in the middle consistently higher in volume than cells at the front or the back (Figure 5D). As these cells had very recently divided and asymmetric cell division is a common mechanism for giving rise to cells of differing size, we sought to identify sibling cell pairs in these images. By imaging several earlier stages (not shown) and incorporating knowledge of the notochord cell lineages, we found that morphogenesis to this point was sufficiently stereotyped that we could identify many, though not all, of the sibling cell pairs (Figure 5C).

The cell pairs pseudocolored in purple were the most anterior cells at an earlier stage and are the descendants of blastomeres A9.10, A9.12 and A9.26. The cells pseudocolored in green are the descendants of blastomeres A9.9 and A9.11. The posterior cell pairs pseudocolored in brown are the secondary lineage notochord cells B9.11 and B9.12, and are the only notochord cells at this stage that have not undergone their final division.

In the anterior notochord, the anteriormost (dark purple) cells were consistently smaller than their posterior (light purple) siblings (volume ratio 45:55, paired sample t-test:6.1×10^{-6}) (Figure 5D). At the posterior end of the notochord, we found the opposite relationship with the posteriormost (dark brown) cells smaller than their more anterior (pale brown) siblings (volume ratio 65:35, paired sample t-test:0.008) (Figure 5D). In the cells near the middle of the notochord where we could identify sib pairs (dark and pale green), a volume asymmetry was not apparent.

It is interesting to note that the most lateral (purple) cells in the 3rd and 4^{th} row show sibling volume asymmetries whereas their more medial (green) neighbors do not. These lateral cell pairs were initially in a more anterior position akin to the first and second rows but were displaced backwards earlier in morphogenesis.

Given that these cells were fixed soon after their last cell division, and given the specific asymmetries observed between different sib pairs, it is likely that these volume asymmetries reflect asymmetric cell divisions. The planar cell polarity (PCP) pathway is known to control many asymmetric cell divisions (Gomes et al., 2009; Lake and Sokol, 2009; Wu and Herman, 2006) and to have diverse roles in ascidian notochord morphogenesis (Jiang et al., 2005; Veeman et al., 2008). Accordingly we examined notochord cell volumes in homozygous *aimless* (*aim*) embryos, which carry a mutation in the core PCP gene *prickle*. The primary notochord lineage in *aim* embryos intercalates extremely slowly and never completes intercalation, whereas the secondary lineage eventually completes intercalation. We thus fixed *aim* and wildtype control embryos relatively late so that we could have a clear linear order of secondary notochord cells (Figures 6A and 6B).

aim embryos show a somewhat less orderly pattern of cell volumes along the AP axis as compared to wildtype, but the basic relationship is still evident (Figures 6C and 6D). By comparing the volumes of cells 1-4 with cells 5-8, we see no difference between *aim* and wildtype embryos in the relative volume of the anteriormost cells as compared to their slightly posterior neighbors (Figure 6E). The same is true at the posterior of the notochord, where we see no difference between *aim* and wildtype embryos in the relative volumes of the anterior 4 secondary notochord cells versus the posterior 4 secondary cells (Figure 6E). While we are not able to identify sibling cell pairs in these embryos, any strong effect on cell volume would be apparent.

For cells in the middle of the notochord where lineage relationships are less clear, we simply compared the histogram distributions of cell volume (Figure 6F). If cell volume asymmetries in this population of cells require PCP signaling, then the distribution of volumes should be narrower. We observe, however, that the distribution is actually slightly broader. These results suggest that PCP signaling is not a major player in generating differential cell volumes in the ascidian notochord, but that it may play a partial role in arranging cells by volume along the AP axis.

We note that notochord cell volumes show a more regular relationship with AP position after intercalation than before. This could represent either local changes in cell volume during intercalation or the intriguing possibility of sorting during intercalation based on volume. 4D timelapse data will likely be required to distinguish between these hypotheses.

Modeling notochord taper

To better understand the relative importance of intercalation timing and cell volume with respect to notochord taper, we constructed several mathematical models. Our first model is based on volume alone. For a hypothetical column of cylindrical cells with uniform height to width ratios, cell radius should vary with the cube root of volume. Figure 7A compares the experimentally observed notochord taper to the taper predicted by the cube root of mean notochord cell volume observed after intercalation. Note that we show taper by the normalized radius as a function of AP cell number, so this model does not involve any assumptions about the precise relationship between cell radius and cell height at any particular time, except that it be uniform along the AP axis. The cube root of volume predicts the overall taper quite well, with a widest point just in front of the AP midpoint and a posterior end that is narrower than the anterior end. It predicts a considerably flatter taper than is actually observed, however, particularly in the front and middle of the notochord.

In quantitative terms, this model suggests that AP differences in cell volume account for at most 63% of observed taper in the anterior of the notochord and 80% percent in the posterior (as measured by root mean square deviation vis-à-vis a hypothetical taperless notochord).

We also built models incorporating the ‘head start’ provided by differential intercalation timing. As shown in Figure 1E, the relative (normalized) radii of cells along the AP axis remain constant as these cells undergo the disk-to-drum cell shape change. This indicates that the rate of change in cell radius is roughly proportional to cell radius, in which case the disk-to-drum transition can be modeled as an exponential decay function with a “halving time” analogous to the half-life in a radioactive decay model. Taper can thus be modeled as:

$$r = r_0 2^{(-h/t_{1/2})}$$

where r is a given cell’s radius at the moment that the entire notochord has completed intercalation, r_0 is the cell’s radius at the moment when that particular cell completes intercalation, h is the head start that cell has before all notochord cells complete intercalation, and $t_{1/2}$ is the halving time.

For a scenario in which intercalation timing is the only mechanism, we held r_0 constant and calculated the predicted taper using experimentally derived values of h and a range of hypothetical halving times. The values of h were estimated from the 50% isocontour of a Loess surface fitted to the heat map of intercalation timing shown in Figure 4D. As shown in Figure 7B, as the halving time increases, the notochord taper asymptotically disappears. As the halving time decreases, the notochord is predicted to be increasingly tapered but the

shape of this taper is quite different from what we observe experimentally. In particular, this model predicts that the anterior should be narrower than the posterior because those cells intercalate first.

In Figure 7C we combine the volume and intercalation timing models by using the cube root of volume as r_0 instead of holding r_0 constant. Here the predicted taper asymptotically approaches the volume-only model as the halving time increases, and becomes more tapered as the halving time decreases. For certain values of $t_{1/2}$, this model predicts an extremely close fit to the observed taper.

For both the timing-only and the timing+volume models, we calculated the $t_{1/2}$ that gave the best fit to the empirically observed taper, as measured by sum squared error. The timing-only model predicted a $t_{1/2}$ of 110 minutes, whereas the timing+volume model predicted a $t_{1/2}$ of 346 minutes. By contrast, when we fit an exponential model to our post-intercalation dataset we estimate that the true $t_{1/2}$ is 203 minutes. At this shorter $t_{1/2}$ the timing+volume model predicts a somewhat more tapered notochord than actually observed.

The above models assume that all 40 notochord cells narrow at the same rate, whereas we have empirically shown that halving times are slightly higher at the anterior and posterior ends (Figure 1F). We incorporated these differential halving times into our model (Figure 7D), and found that it provided a good fit to the experimentally observed notochord taper. Note that this model had no free parameters. It used only measured values for cell volume, the timing of when intercalation finished, and the rate of the disk-to-drum transition to predict the taper.

We also quantified how well these various predicted notochord tapers fit the observed taper, as measured by sum squared error (Figure 7E). The timing only model performs relatively poorly with either an empirically derived $t_{1/2}$ value or the $t_{1/2}$ value giving the best result. The volume only model, which has no free parameters, performs relatively well. The volume+timing model improves upon this, both for the best $t_{1/2}$ and the empirically derived $t_{1/2}$. When we include empirical $t_{1/2}$ values that vary from cell to cell instead of using a mean value for all cells, the fit is modestly improved compared to using the empirically derived mean value.

The best fit is obtained, however, using the timing+volume model and a $t_{1/2}$ of 346, which is ~70% higher (narrows more slowly) than what we actually observe. A potential explanation for this is that the notochord could be somewhat flatter at each cell's r_0 than predicted by the cube root of volume, so that somewhat more of the overall taper comes from timing versus volume. Our estimates of r_0 for cells 3, 16 and 38 in Figure 4 suggest that this is likely correct.

We conclude from these measurements and models that both cell volume and the timing and kinetics of the disk-to-drum transition are essential to explaining notochord taper. While this simple geometrical model does not incorporate the biomechanics of intercalation and the disk-to-drum transition, it does suggest that the cellular mechanisms described here are largely sufficient to explain the intercalated notochord's tapered shape.

Discussion

The simple embryonic architecture of ascidians, such as *Ciona*, provides a unique model for working towards a systems biology of morphogenesis. In the case of the notochord, 40 post-mitotic cells intercalate into a tapered 1×40 rod. While a considerable amount is known about the mechanisms of cell intercalation in the notochord, no consideration has previously been given to the mechanisms controlling its taper.

We show here that *Ciona* notochord taper reflects three main mechanisms: unequal partitioning of cell volume, which influences the width of each cell at the time it finishes intercalation; the timing of intercalation, whereby cells at the ends start the disk-to-drum transition earlier than cells in the middle; and the kinetics of the disk-to-drum transition, which is slower at the ends than in the middle. Note that these latter two mechanisms are acting at cross-purposes to one another, with the ends-to-middle progression of intercalation acting to increase notochord taper whereas the longer $t_{1/2}$ at the ends of the notochord acts to slightly decrease taper. We speculate that being wider in the middle than at the ends should be extremely robust given these multiple mechanisms, but also that there are many points at which natural selection could act to fine-tune notochord taper.

Sibling cell asymmetries are usually thought of in terms of the segregation of cell fates, but here we have shown that they can play an important role in organ shape through the control of cell volume. The fine-grained control of cell volume may be most relevant to morphogenesis in organs, such as the *Ciona* notochord, with a relatively small number of cells. Spatial and temporal subtleties of cell intercalation are likely relevant, however, to many tapering structures. It will be interesting to know if similar mechanisms contribute to notochord taper in other chordates, or to taper in other embryonic contexts. It should be possible to extend methods for *in toto* 3D cell morphometry to give quantitative information about many aspects of morphogenesis.

It remains unclear what signaling mechanisms control sibling cell volume asymmetries in the ascidian notochord, though PCP signaling does not appear to be a major contributor. A series of asymmetric divisions in the posteriormost cells of early cleavage stage embryos are known to involve a cytoplasmic determinant called the Centrosome Attracting Body (CAB) (Nishikata et al., 1999). The CAB is not thought to be involved in notochord morphogenesis, although this is difficult to formally test as CAB function is required for the initial induction of the notochord.

Many structures in nature display a tapered morphology, and there are likely strong adaptive and biophysical reasons for these shapes. The taper of cat whiskers, for example, is thought to be important for the mechanics of tactile sensation (Williams and Kramer, 2010), whereas the tapered body plan of many fish is thought to be important for efficient swimming (McMillen and Holmes, 2006; McMillen et al., 2008). The *Ciona* tail tapers only to the posterior whereas the notochord tapers to both the anterior and the posterior, so it is likely that hydrodynamic streamlining is not the only functional consideration. For chordates with swimming larval stages (or swimming adult stages with persistent notochords), the notochord has important mechanical properties as an elastic beam acting in compression against tension from the bilateral musculature of the trunk and tail (Long et al., 2002; McHenry and Patek, 2004). We speculate that notochord taper may be important for mechanical properties such as resonance, deflection or damping.

Supplementary Material

Refer to Web version on PubMed Central for supplementary material.

Acknowledgments

This work was supported by grant HD059217 from the NIH to WCS and B.S. Manjunath.

References

Carpenter AE, et al. CellProfiler: image analysis software for identifying and quantifying cell phenotypes. Genome Biol. 2006; 7:R100. [PubMed: 17076895]

Dong B, et al. Distinct cytoskeleton populations and extensive crosstalk control Ciona notochord tubulogenesis. Development. 2011; 138:1631–41. [PubMed: 21427145]

Dong B, et al. Tube formation by complex cellular processes in Ciona intestinalis notochord. Dev Biol. 2009; 330:237–49. [PubMed: 19324030]

Dufour A, et al. Segmenting and tracking fluorescent cells in dynamic 3-D microscopy with coupled active surfaces. IEEE Trans Image Process. 2005; 14:1396–410. [PubMed: 16190474]

Gomes JE, et al. Van Gogh and Frizzled act redundantly in the Drosophila sensory organ precursor cell to orient its asymmetric division. PLoS One. 2009; 4:e4485. [PubMed: 19214234]

Hotta K, et al. A web-based interactive developmental table for the ascidian Ciona intestinalis, including 3D real-image embryo reconstructions: I. From fertilized egg to hatching larva. Dev Dyn. 2007; 236:1790–805. [PubMed: 17557317]

Jiang D, et al. Ascidian prickle regulates both mediolateral and anterior-posterior cell polarity of notochord cells. Curr Biol. 2005; 15:79–85. [PubMed: 15700379]

Kroon, DJ.; Slump, CH. Coherence Filtering to Enhance the Mandibula Canal in Cone-Beam CT Data. Proceedings of the 4th Annual Symposium of the IEEE-EMBS Benelux Chapter; 2009. p. 41-44.

Lake BB, Sokol SY. Strabismus regulates asymmetric cell divisions and cell fate determination in the mouse brain. J Cell Biol. 2009; 185:59–66. [PubMed: 19332887]

Long JH Jr. et al. The notochord ofhagfish Myxine glutinosa: visco-elastic properties and mechanical functions during steady swimming. J Exp Biol. 2002; 205:3819–31. [PubMed: 12432006]

McHenry MJ, Patek SN. The evolution oflarval morphology and swimming performance in ascidians. Evolution. 2004; 58:1209–24. [PubMed: 15266971]

McMillen T, Holmes P. An elastic rod model for anguilliform swimming. J Math Biol. 2006; 53:843–86. [PubMed: 16972099]

McMillen T, et al. Nonlinear muscles, passive viscoelasticity and body taper conspire to create neuromechanical phase lags in anguilliform swimmers. PLoS Comput Biol. 2008; 4:e1000157. [PubMed: 18769734]

Meyer F, Beucher S. Morphological segmentation. J. Visual Commun. Image Represent. 1990; 1:21–46.

Miyamoto DM, Crowther RJ. Formation of the notochord in living ascidian embryos. J Embryol Exp Morphol. 1985; 86:1–17. [PubMed: 4031734]

Montell DJ. Morphogenetic cell movements: diversity from modular mechanical properties. Science. 2008; 322:1502–5. [PubMed: 19056976]

Munro E, et al. Cellular morphogenesis in ascidians: how to shape a simple tadpole. Curr Opin Genet Dev. 2006; 16:399–405. [PubMed: 16782323]

Munro EM, Odell GM. Polarized basolateral cell motility underlies invagination and convergent extension of the ascidian notochord. Development. 2002; 129:13–24. [PubMed: 11782397]

Nishida H. Cell lineage analysis in ascidian embryos by intracellular injection of a tracer enzyme. III. Up to the tissue restricted stage. Dev Biol. 1987; 121:52641.

Nishikata T, et al. The centrosome-attracting body, microtubule system, and posterior egg cytoplasm are involved in positioning of cleavage planes in the ascidian embryo. Dev Biol. 1999; 209:72–85. [PubMed: 10208744]

Paluch E, Heisenberg CP. Biology and physics of cell shape changes in development. Curr Biol. 2009; 19:R790–9. [PubMed: 19906581]

Sherrard K, et al. Sequential activation of apical and basolateral contractility drives ascidian endoderm invagination. Curr Biol. 2011; 20:1499–510. [PubMed: 20691592]

Stemple DL. Structure and function of the notochord: an essential organ for chordate development. Development. 2005; 132:2503–12. [PubMed: 15890825]

Tassy O, et al. A quantitative approach to the study of cell shapes and interactions during early chordate embryogenesis. Curr Biol. 2006; 16:345–58. [PubMed: 16488868]

Thomas N. High-content screening: a decade of evolution. J Biomol Screen. 2009; 15:1–9. [PubMed: 20008124]

Veeman MT, et al. Ciona genetics. Methods Mol Biol. 770:401–22. [PubMed: 21805273]

Veeman MT, et al. Chongmague reveals an essential role for laminin-mediated boundary formation in chordate convergence and extension movements. Development. 2008; 135:33–41. [PubMed: 18032448]

Vincent L, Soille P. Watersheds in digital spaces: An efficient algorithm based on immersion simulations". IEEE PAMI. 1991; 13:583–598.

Weickert J. Coherence-Enhancing Diffusion Filtering. International Journal of Computer Vision. 1999; 31:111–127.

Williams CM, Kramer EM. The advantages of a tapered whisker. PLoS One. 2010; 5:e8806. [PubMed: 20098714]

Wu M, Herman MA. A novel noncanonical Wnt pathway is involved in the regulation of the asymmetric B cell division in C. elegans. Dev Biol. 2006; 293:31629.

Zanella C, et al. Cells segmentation from 3-D confocal images of early zebrafish embryogenesis. IEEE Trans Image Process. 2009; 19:770–81. [PubMed: 19955038]

Highlights

-Multiple mechanisms control the tapered shape of the ascidian notochord.

-Sibling cell volume asymmetries affect cell diameter along the AP axis.

-Cells at the ends intercalate first, giving them a head start on subsequent narrowing.

-Small AP differences in the rate of narrowing help to fine-tune the taper.

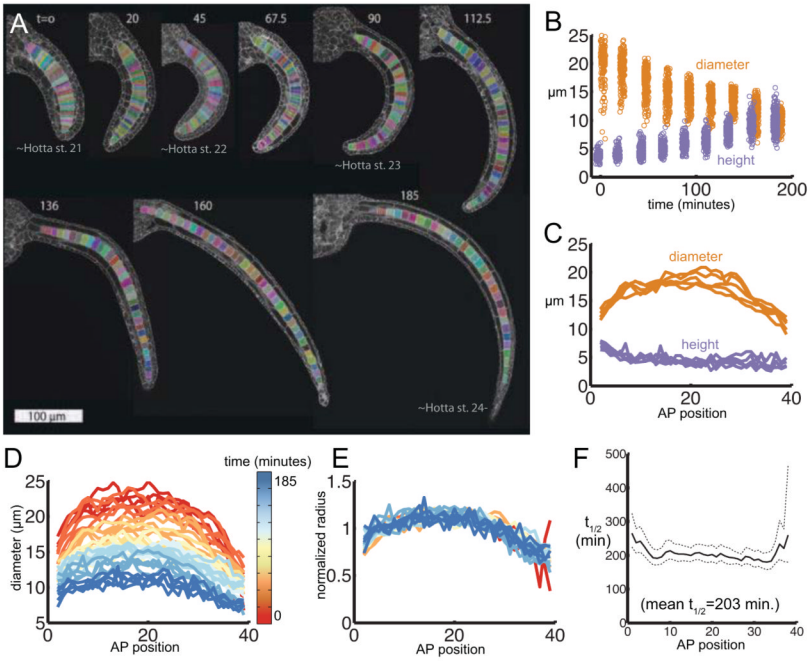

Figure 1. The *Ciona* notochord is tapered

(A)Mid-notochord confocal planes of representative phallacidin-labeled *Ciona savignyi* embryos at the indicated timepoints (minutes). Phallacidin labels the actin cytoskeleton, which is largely cortical at these stages. Segmented notochord cells are shown as a randomly pseudocolored overlay. (B) Notochord cell height (purple) and diameter (orange) as a function of time. Values have been jittered slightly for display purposes. (C) Notochord cell height (purple) and diameter (orange) as a function of AP position in the notochord for 5 embryos at the 45 minute timepoint. (D) Notochord cell diameter as a function of AP position. All timepoints are shown, pseudocolored from youngest (red) to oldest (blue). (E) Relative (normalized) cell diameter. Each notochord cell's diameter was normalized to the mean diameter of that particular notochord to indicate cells consistently wider than average (>1) and narrower than average (<1). All timepoints collapse onto a similar curve. (F) Experimentally observed halving times (X axis) as a function of AP position (Y axis) obtained by fitting exponential curves to the post-intercalation dataset on an AP cell-by-cell basis. The dashed lines indicate 95% confidence intervals.

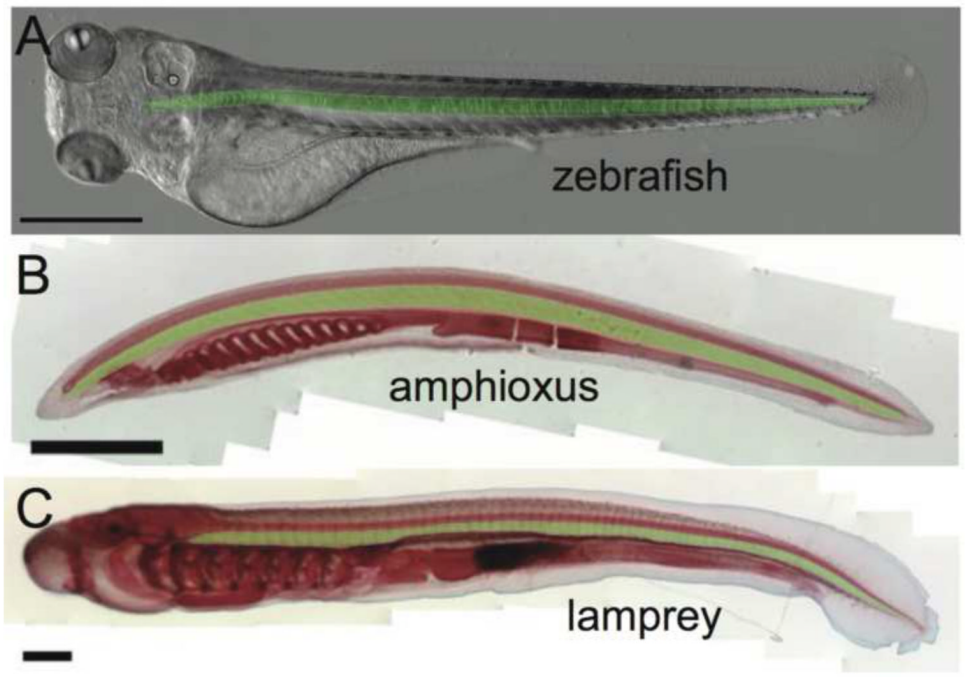

Figure 2. The ubiquity of taper

(A-C) Larval stages of (A) zebrafish, (B) amphioxus and (C) lamprey with the notochord pseudocolored in green. In all cases, the notochord is tapered towards the anterior and the posterior.

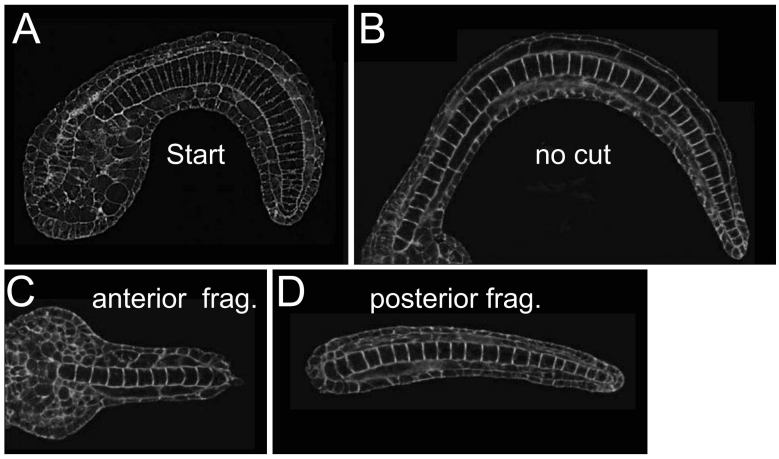

Figure 3. Tail cutting experiments

(A) Unperturbed control embryo (0 min). (B) Unperturbed control embryo (120 min.). (C) Representative anterior fragment from an embryo bisected at ~0 minutes and fixed at 120 minutes. (D) Representative posterior fragment from an embryo bisected at ~0 minutes and fixed at 120 minutes.

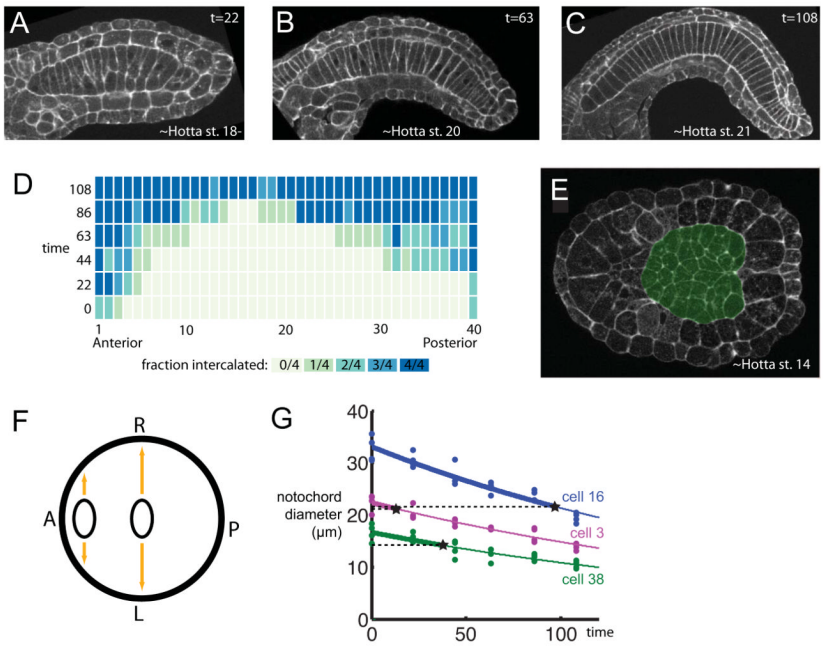

Figure 4. Intercalation timing and notochord diameter

(A-C) Representative images from 3 of the 6 stages of notochord cell intercalation examined. (D) Heat map of intercalation timing incorporating data from 4 embryos at each of 6 stages. The color indicates the fraction of embryos in which a particular cell was found to have completed intercalation at a given timepoint. (E) The notochord primordium (pseudocolored green) at the onset of notochord cell intercalation is in the shape of a disk. (F) Cartoon diagram showing how a cell at the front of a disk-shaped notochord primordium has less far to travel to complete intercalation than a cell near the middle. (G) Diameter of the entire notochord at three AP positions: anterior (cell 3, magenta), middle (cell 16, blue) and posterior (cell 38, green). An exponential model is fitted to each set of points. The point on each regression line at which that cell has a 50% probability of having completed intercalation is shown with a star, and provides an estimate of mean width (dotted line) at the moment when that cell completes intercalation.

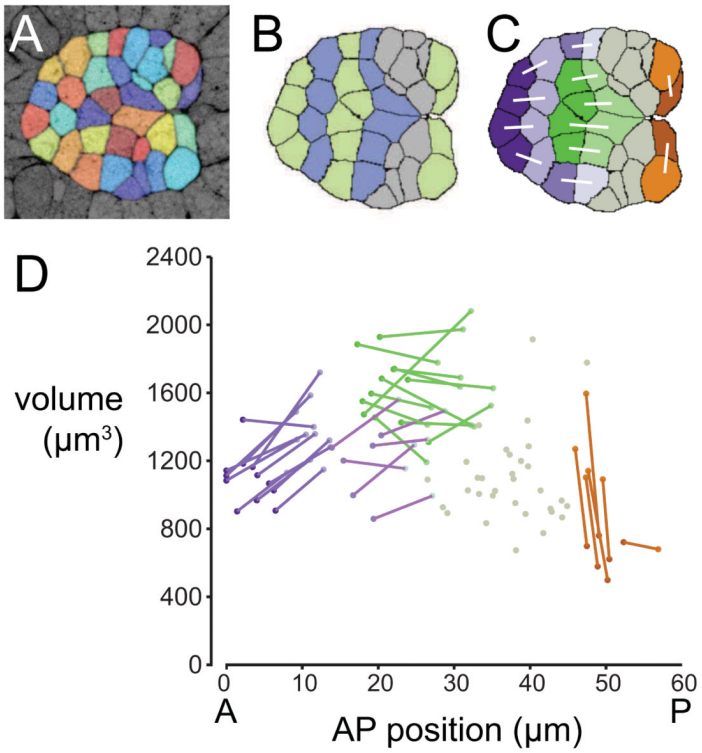

Figure 5. Sibling cell volume asymmetries in the preintercalation notochord

(A)The disk-shaped notochord primordium at the onset of intercalation. Cell segmentations are overlayed as random pseudocolors on top of the original data. Anterior is to the left. Right is to the top. (B) The same segmentation recolored to emphasize the regular pattern of notochord cells at this timepoint, with anterior rows of 4, 4, 6 and 6 cells, and 4 distinctive cells at the posterior. The cells marked in gray were less obviously stereotyped at this timepoint. (C) The same segmentation relabeled by cell lineage with known sister cells connected by white lines. (D) Cell volume as a function of AP position for 3 segmented notochord primordia (AP position given as μm from the centroid of the most anterior cell). Cells are labeled according to the map in (C) and sibling cells are connected with lines.

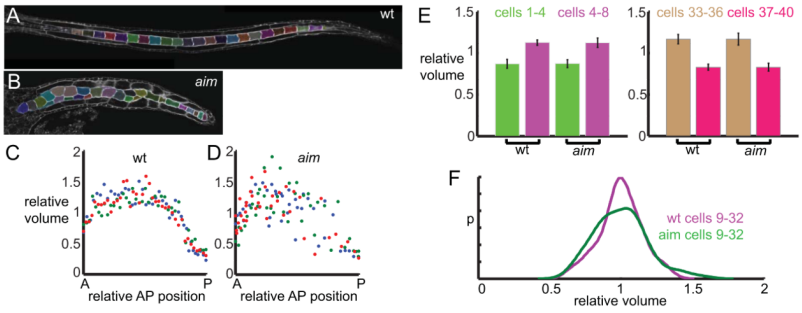

Figure 6. Cell volumes in wildtype and *aim* embryos

(A, B) Representative images of segmented notochord cells in (A) wildtype and (B) *aim*/*aim* embryos. (C, D) Cell volume as a function of AP position in (C) wildtype and (D) *aim*/*aim* embryos. As *aim* embryos are much shorter than wildtype, AP position is normalized to the length of each notochord. Data points for each of 3 segmented notochords for each genotype are labeled different colors. (E) Relative cell volumes for cells 1-4 (green) versus 5-8 (magenta), and cells 33-36 (brown) versus 37-40 (red). We observed some intermingling of primary and secondary notochord cells in *aim*/*aim* but not wildtype embryos, so for this assay, we defined cells 33-36 as the anteriormost 4 of the 8 secondary notochord cells and cells 37-40 as the posteriormost 4 of the 8 secondary notochord cells. The secondary cells were always distinguishable by their lower volume. Error bars show the standard error of measurement. (F) Kernel density estimate histogram of relative cell volumes for cells 9-32 in wildtype (magenta) and *aim* (green) embryos.

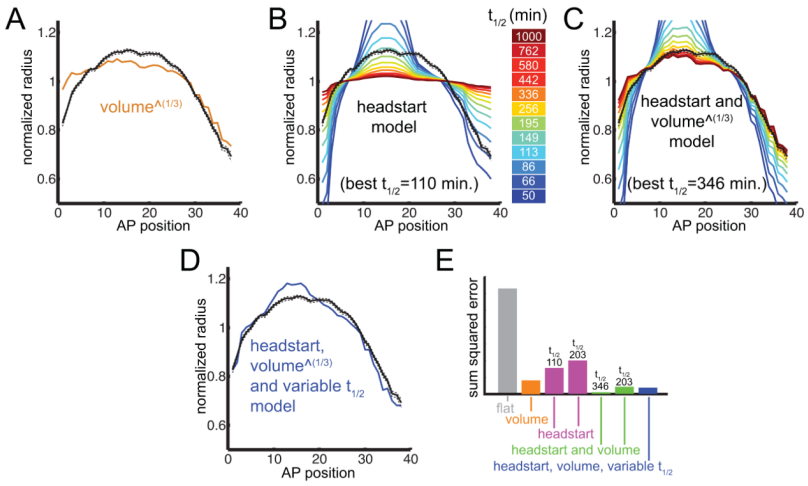

Figure 7. Modeling notochord taper

(A, B, C, D) Normalized taper (Y axis) as a function of AP position (X axis). The mean taper experimentally observed is shown with a solid black line to compare with various models. The dashed black lines are +/− standard error of measurement (A) Volume-only model, using the cube root of mean post-intercalation cell volume. (B) Timing-only model for a log-spaced series of halving times indicated with the color legend. (C) Timing+volume model using the same coloring scheme as (B). (D) Timing+volume+variable $t_{1/2}$ model. (E) Bar graph of sum squared errors for each model compared to mean observed taper.